The Effect of ECM Stiffness on Tip/Stalk Cell Patterning during Early Sprouting Angiogenesis

A computational approach

B.M. Waasdorp

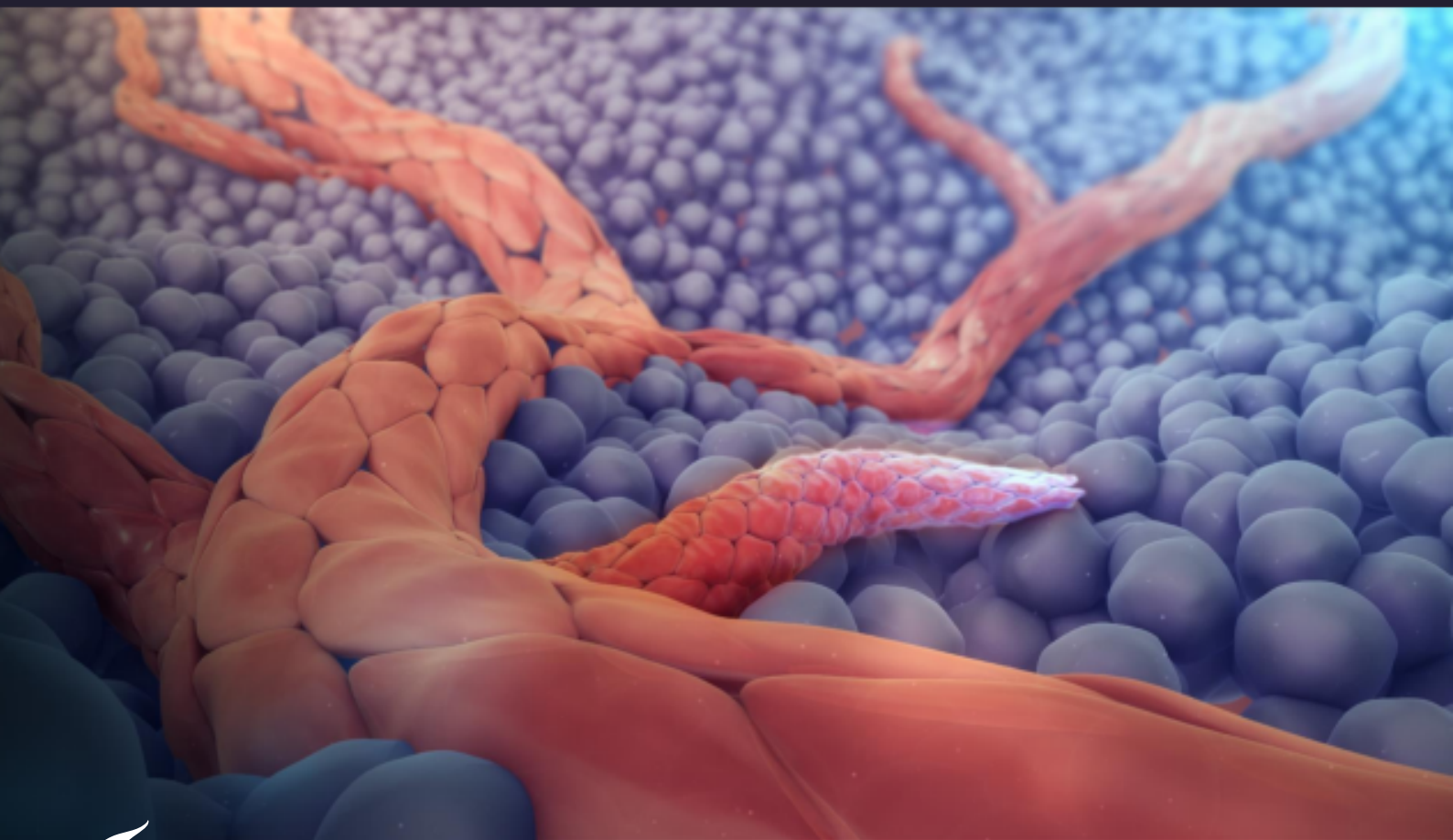

TU Delft

The Effect of ECM Stiffness on Tip/Stalk Cell Patterning during Early Sprouting Angiogenesis

A computational approach

by

B.M. Waasdorp

to obtain the degree of Master of Science
at the Delft University of Technology,
in Applied Mathematics,
to be defended publicly on Wednesday February 28, 2024 at 9:30 AM.

Student number:	4572114	
Project duration:	October 10, 2022 – February 28, 2024	
Thesis committee:	Dr. J. L. A. Dubbeldam,	TU Delft, first supervisor
	Dr. ir. E. G. Rens,	TU Delft, second supervisor
	Prof. dr. ir. M. B. van Gijzen,	TU Delft
	Prof. dr. S. Checa Esteban,	Julius Wolff Institute, external supervisor

Cover: Angiogenesis - New blood vessels forming from pre-existing vessels. [1]

TU Delft

JULIUS WOLFF INSTITUT
BIH Center for Musculoskeletal Biomechanics and Regeneration

Preface

This thesis is executed at the Julius Wolff Institute - Center for Musculoskeletal Biomechanics and Regeneration in Berlin. It employs a computational approach to investigate the impact of extracellular matrix stiffness on tip/stalk cell patterning during the early stages of sprouting angiogenesis. This aims to bridge the literature gap concerning mechanical cues coming from the environment surrounding vessels and their impact on the initial step in vascular formation - tip cell selection. A deeper understanding on this topic holds clinical relevance, particularly in the context of bone or wound healing, as well as in anti-angiogenic treatment strategies for cancer.

I would like to sincerely thank Johan Dubbeldam and Lisanne Rens for their guidance, involvement and genuine interest in the project. Their combined experience and expertise in the field served as a constant source of motivation and taught me a lot throughout this thesis.

Furthermore, I would like to thank Sara Checa for her guidance at the Julius Wolff Institute, where she ensured to keep me on the right track and provided me with opportunities to present my research beyond the institute as well. Engaging in discussions on such a specialized topic outside the field of mathematics was a uniquely enriching experience.

I want to acknowledge the whole Computational Mechanobiology group for creating a friendly and supporting environment, where everyone was eager to help each other out in their research. Here I would like to give a very special thank you to Chiara Dazzi, who throughout the entire period of the thesis project stood by my side on both a professional and personal level. At any time, she was happy to engage in collaborative brainstorming to help me navigate and come up with solutions for the challenges I encountered.

Lastly, my gratitude extends to my family and friends for supporting me in this academic journey abroad, even from a distance.

B.M. Waasdorp
Berlin, February 2024

Summary

Angiogenesis, the process by which new vessels sprout off from existing ones, is relevant in many physiological processes such as bone or wound healing. Impaired angiogenesis can impede the delivery of oxygen and nutrients to the injured site, hindering the healing process. Conversely, in tumor development, inhibiting angiogenesis may be a desired therapeutic strategy.

In the initial phase of sprouting angiogenesis, tip cells are selected to branch from the existing blood vessel. Stalk cells follow behind the tip cell and proliferate to form the vessel wall. Despite several experimental studies and mathematical models that have attempted to investigate the signaling pathways responsible for tip cell selection, a notable gap exists in the literature regarding the effect of extracellular matrix (ECM) stiffness on this process. This is of clinical interest since changes in stiffness occur during various physiological and pathological processes. This thesis aims to address this gap by investigating the specific influence of ECM stiffness on tip/stalk cell patterning.

A computational model for VEGF-mediated cell patterning was developed to explore the intricate interplay between mechanical cues from the ECM stiffness and the signaling pathways governing tip cell selection during sprouting angiogenesis. Building upon the model proposed by Venkatraman et al. [24], this extension incorporates the influence of ECM stiffness on key protein concentrations within endothelial cells.

The computational model built in this thesis simulates a vessel sprout under the stimulus of a dynamic VEGF gradient field. The model was calibrated against experimental data and predicts cell patterning outcomes across varying ECM stiffness levels. An alternating pattern of tip and stalk cells (salt-and-pepper pattern) was predicted, indicating a desired angiogenic response. However, when ECM stiffness surpassed a certain threshold, this patterning failed. The abrupt transition from a clear salt-and-pepper pattern to complete pattern failure can be attributed to the signaling pathways' character that amplifies small variations between cells. This could be clarified by tracking the concentration levels of Delta-like-ligand 4 (Dll4), the bounded Notch receptor and the VEGF receptor (VEGFR2). Furthermore, in accordance with existing literature [14], the model predicted that a rise in ECM stiffness induces a faster pattern process, hinting at the formation of denser vascular networks. However, this accelerated patterning was impeded in excessively stiff environments, indicating the formation of a sparser network.

In this thesis, additional studies have been performed to investigate more in depth the influence of the sensitivity of filopodia-mediated VEGF sensation and the VEGF binding rate on cell patterning. First, cell patterning was investigated across various parameter choices for the filopodia-mediated VEGF sensation function, simulating a low to high sensitivity to a rise in filopodia. This approach aimed to account for factors that are situation dependent in real-world conditions. These factors entail ECM stiffness, filopodia length, or the VEGFR2 distribution on filopodia. A higher sensitivity in VEGF sensation resulted in a faster patterning process, which is consistent with the literature [26]. However, an excessively high sensitivity weakens the opposite cell states. Concerning ECM stiffness, the model's predictions revealed a pattern failure in less stiff environments for a higher sensitivity of filopodia-mediated VEGF sensation.

Second, the VEGF binding rate was modulated to simulate angiogenic treatments based on reduced VEGF binding or increased VEGFR2 internalization. Simulations incorporating a higher binding rate demonstrated stronger opposite cell states, creating favourable conditions for pro-angiogenic treatments in for example, bone healing. However, the stiffness level at which the pattern failed was lower compared to simulations with a low binding rate. While further experimental data is essential to validate this result, it already underscores the importance of accounting for ECM stiffness in the exploration of angiogenic treatments based on VEGF binding.

To further develop the model, the Notch cleavage after binding with Dll4 was integrated into the equations governing the signaling pathways. This allowed to better fit experimental data and led to pattern failure occurring at significantly lower ECM stiffness levels compared to simulations that exclude Notch cleavage. While this finding underscored the potential importance of including Notch cleavage in analyzing cell patterning within an ECM stiffness-dependent context, caution is essential in drawing

definite conclusions from this model. A more extensive parameter study is crucial to fully understand the effects resulting from the inclusion of Notch cleavage on tip/stalk cell patterning.

In summary, the computational model presented in this thesis incorporates the effect of ECM stiffness on tip/stalk cell patterning, stressing its importance in the investigation of angiogenic treatments. While predictions reliant on ECM stiffness need additional experimental data for validation, it is evident that changes in stiffness impact cell patterning and, consequently, the course of sprouting. Continued refinement of the model holds great promise for deepening the understanding of angiogenic processes and the exploration of treatment strategies.

Contents

1 Introduction

1.1. Clinical motivation

The formation of blood vessels from already existing ones, called angiogenesis, is an important physiological process. In bone or wound healing, the expansion of vascularization is needed to bring enough oxygen and nutrients to the injured site and to remove waste products, allowing a successful healing process. Several studies have found that impaired angiogenesis slows healing down or may even fully prevent it [6, 9]. In tumor development, this might be a desired response, as it blocks the blood flow towards the tumor, which inhibits its growth.

Sprouting angiogenesis is regulated by both biochemical and mechanical signals in the environment surrounding vessel cells [7]. Although many studies have investigated sprouting angiogenesis and the role of mechanical and chemical signals in sprout patterning, the interaction between both these signals and their effect on sprout patterning remains poorly understood.

The tissue surrounding vessel cells vary in stiffness, depending on whether it is healthy or diseased, or more specifically the stage of healing. Including mechanical cues from the stiffening environment into a computational model to study its effect on sprouting angiogenesis could aid in choosing the optimal biomaterials in regenerative therapy, or in choosing anti-angiogenic treatments in cancer. Therefore, it is of importance to investigate the role these mechanical stimuli have on the signaling pathways involved in vessel patterning.

1.2. Background

1.2.1. Signaling pathways regulate cell patterning

The interior of a blood vessel is lined by a layer of endothelial cells (ECs), which proliferate and migrate in order to expand the existing vessel network (i.e., sprouting). In each endothelial cell, several proteins interact with each other through so-called signaling pathways, which determine the function of this cell. These pathways within a cell receive signals by interacting with neighbouring cells, as well as through interaction with its environment.

When the body senses a lack of oxygen (hypoxia), vascular endothelial growth factors (VEGFs) are released. These growth factors are a call to the endothelial cells to form new sprouts so that the site can be supplied with oxygen again. Filopodia extend endothelial cells to sense their environment, so that more VEGFs can bind to their receptor (VEGFR2). This sets the sig-

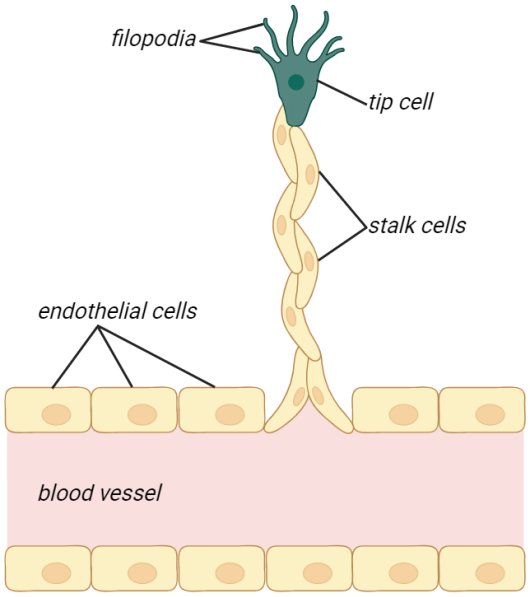

Figure 1.1: From a pre-existing blood vessel, a tip cell is selected which forms filopodia. The tip cell breaks out of the vessel barrier, where proliferating stalk cells follow behind to form the sprout.

naling pathways in motion and endothelial cells differentiate to fulfill different functions, causing them to differ in mostly migratory and proliferation behaviour. The tip-cell phenotype branches from the existing vessel and has a high migratory character due to its long filopodia to lead the sprout (primarily) towards the VEGF gradient. The stalk-cell phenotype proliferates and follows behind the tip-cell, forming the new blood vessel (Fig. 1.1).

1.2.2. Lateral inhibition ensures alternating tip and stalk cells

The differentiation of endothelial cells into tip or stalk cells is regulated mainly by the Notch signaling pathway. This pathway uses lateral inhibition to ensure there will not be two adjacent tip cells, but alternates tip and stalk cells into a salt-and-pepper pattern [2] (Fig. 1.2). This specific patterning is crucial for a good angiogenic response. In the case of an excess of tip cells, hypersprouting occurs, in which the many branches are too fragile and insufficiently organized and are therefore nonfunctional [5]. Conversely, too few tip cells lead to a vascular network too sparsely configured to sustain sufficient blood supply [23]. Therefore, a comprehensive understanding of tip/stalk cell patterning is vital to ensure successful angiogenesis.

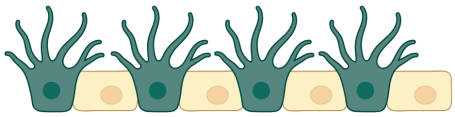

Figure 1.2: Notch signaling makes sure that endothelial cells fall in a salt-and-pepper pattern of alternating tip (green) and stalk (yellow) cells.

Lateral inhibition is achieved through binding of Delta-like-ligand 4 (Dll4) to the Notch receptor presented on a neighbouring cell. This binding event activates the Notch receptor, leading to the release of the Notch intracellular domain (NICD). Subsequently, the NICD translocates to the cell nucleus and causes the expression of target genes HES, HEY and HER (HE). These genes, in turn, suppress the expression of VEGFR2, decreasing the binding to VEGFs. VEGF binding is needed for the formation of filopodia, and so for the ability of a cell to sense the growth factors. In essence, the combination of Notch signaling between cells and the ongoing feedback loop between VEGF uptake and filopodia formation are responsible for the cell patterning. These two factors should be in good balance in order to establish the desired opposite cell states (tip and stalk). An overview of these connections is shown in figure 1.3.

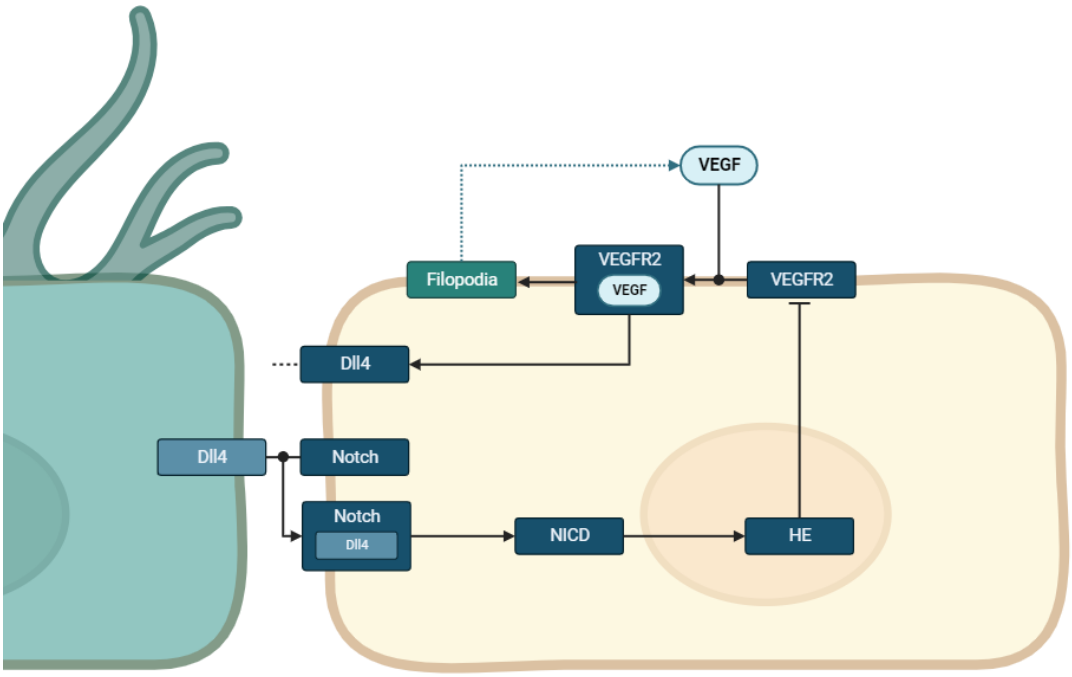

Figure 1.3: Interactions of the VEGF-induced Notch signaling pathway in an endothelial cell. The filled circles represent binding. The black arrowheads represent upregulation and the stripe heads represent inhibition. The blue, dotted arrow represents the sensation of VEGF by filopodia. HE is the collective name of HES, HEY and HER.

1.2.3. Role of mechanical signals on sprouting angiogenesis

Several mechanical cues, such as extracellular matrix (ECM) deformations, pulling forces from neighbouring cells, or shear stress induced by blood flow, can alter the cell patterning. Most of these cues come from the ongoing matrix deformations that change ECM stiffness and density [15]. The ECM is a network of proteins and molecules that surrounds and supports the endothelial cells. In many processes like tumor development and wound healing the ECM stiffens, thereby influencing the vessel growth and branching [8]. It has been reported that an increase in ECM stiffness supports sprouting and migration. However, when the stiffness gets too high, network formation can be completely prevented [8, 14].

The ECM stiffening alters the cell morphology and, via mechanotransduction, the signaling pathways dictating its phenotype. Matsuo et. al. found through an *in vitro* study that in stiffer environments Dll4 expression is suppressed through the activation of the mechanotransducing protein YAP [17]. Furthermore, Kretschmer et. al. found that a stiffer ECM may decrease the intercellular binding of the Notch receptor with its ligand [15]. It is of significance to explore the effect of these two findings on the cell patterning, in order to understand the way the ECM stiffening contributes to sprouting angiogenesis.

1.3. State of the art on mathematical models of angiogenesis

Due to the complexity of the process, mathematical models have been a powerful tool to investigate the interactions between the different signaling molecules and their influence on tip/stalk patterning.

Prokopiou et al. [20] deployed an ODE system, describing lateral inhibition in a simple form, where available VEGF, modeled through a gradient field, upregulates Dll4, subsequently activating Notch in adjacent cells. Conversely, Notch inhibits Dll4 within the same cell. A tip cell is defined to have Dll4 concentration above a specified threshold. This ODE system is coupled to a cell-based model, which allows for investigation of cell-level properties such as cell-cell adhesion or cell-ECM contact guidance.

Palm et al. [19] integrated a system of ODEs with a cell-based model, wherein the reactions governing cell patterning include the release of NICD following the binding of Dll4 to the Notch receptor. The cell is characterized as tip when the NICD concentration is below a designated threshold.

Bentley et al. [2] created an agent-based model that not only accounts for Notch-binding, but also simulates filopodia extension and retraction. The lateral inhibition process is now enhanced by a pos-

itive feedback loop, wherein filopodia function as sensors, enhancing VEGF uptake. A cell attains tip cell status when filopodia surpass a designated threshold and the cell has not yet undergone lateral inhibition from neighbouring cells.

Venkatraman et al. [24] formulated a mathematical model where this positive feedback is captured in a non-spatial manner. The reactions responsible for lateral inhibition are modeled more comprehensively (Fig. 1.3). With this model they investigated the time required for two cells to select which becomes the tip cell, defined by Dll4 surpassing a threshold. Page et al. [18] coupled this mathematical model to the agent-based model by Bentley et al. and found that the VEGF-driven positive feedback speeds up the tip/stalk cell patterning. In fact, it generates a sensitive switch wherein minor discrepancies are amplified to yield the opposite cell states, tip and stalk.

Kühn and Checa made a more detailed mathematical model for tip cell selection [16], considering not only VEGFR2 but VEGFR1 as well. Cis-inhibition, i.e. the inhibition of Dll4 and Notch when binding within the same cell, is included too. Previously investigated by Sprinzak et al. [21], this mechanism should enhance the lateral inhibition process as well. Additionaly, Kühn and Checa introduced a time delay by describing the transcription and translation as individual time processes for each protein. This intricate model is coupled to an agent-based model to simulate the formation of the vascular network. In each update, the mathematical model selects whether cells become a tip or a stalk cell. A cell is identified as tip when Dll4 and filopodia exceed a specified threshold and the VEGFR2 concentration is greater than that of VEGFR1. If a cell satisfies these tip cell criteria, it migrates and a stalk cell is placed in tip cells' old position, modeling their proliferative behavior. This coupling to the agent-based model allows for a better prediction of sprouting angiogenesis within a dynamic context.

Over the course of research, mathematical models describing tip cell selection have evolved to become more comprehensive. Some have extended to multiscale models, enabling the correlation of tip/stalk cell patterning with network formation. However, the previous models have not addressed the interplay between mechanical and chemical signals.

Koon et al. [13] introduced a mechanical aspect to a lateral inhibition model by hypothesizing a tension-dependent Delta-Notch binding rate. This contributed to a more realistic recreation of tip/stalk cell patterning.

Nevertheless, there remains a gap in our understanding of how mechanical signals precisely impact Notch signaling. This thesis aims to address this gap by initiating an investigation into the role of extracellular matrix stiffness.

1.4. Research objectives

The overall goal of this thesis is to integrate ECM stiffness into a mathematical model that describes the intricate signaling pathways that govern tip cell selection. Integrating this into a computational model allows to examine the impact of varying ECM stiffness on tip/stalk cell patterning in a vessel sprout under a VEGF stimulus. The main research question in this thesis is as follows:

"How do mechanical cues coming from ECM stiffness affect the tip/stalk cell patterning during early sprouting angiogenesis?"

In examining the main question, four research objectives have been formulated.

1. *"How does ECM stiffness alter protein expression in the signaling pathways involved in tip-cell selection?"*
   In this thesis, the model of Venkatraman et al. describing the VEGF-mediated Notch signaling pathway [24] is extended to take into account the influence of the surrounding ECM stiffness on the signaling pathways involved. A first objective is to zoom in inside the cell and investigate the alterations of the relevant protein concentrations.
2. *"How does filopodia-mediated VEGF sensation influence the cell patterning in varying stiffness environments?"*
   In this work, a dynamic VEGF gradient field is modeled to simulate active filopodia sensation, in contrast to Venkatraman's model, in which a static input was used. This work adjusts the function describing filopodia-mediated VEGF sensation, now accounting for dynamic inputs to provide a more realistic simulation.
   The degree in which filopodia can sense VEGF is very situation dependent. As filopodia navigate

along ECM fibers, their sensing capability is intricately tied to ECM properties, such as the stiffness [11]. Furthermore, factors like filopodia length or the distribution of the VEGF receptors on the filopodia affect their sensing ability as well. Being aware of these diverse factors, it is crucial to explore a range of function choices and investigate their effect on the cell patterning in varying stiffness environments.

3. *"How is the cell patterning affected by therapeutic modulation of VEGF binding under various stiffness conditions?"*
   The VEGF binding will be modulated to simulate angiogenic treatments based on reduced VEGF binding or increased VEGFR2 internalization [12, 10]. Such anti-angiogenic treatments hold potential to block the blood flow to tumors, thereby inhibiting their growth. Conversely, pro-angiogenic treatments could be used to increase the chance of bone healing. However, how different ECM stiffness levels impact these treatments is not known and will therefore be investigated.
4. *"How does inclusion of the Notch cleavage change the patterning behavior for different levels of ECM stiffness?"*
   The model of Venkatraman will be further developed to include the cleavage of the bounded Notch receptor to investigate its influence on cell patterning over various stiffness levels.

1.5. Thesis outline

To investigate the main question, a computational model for VEGF-mediated cell patterning is built. An overview of the methodology is given in section 2. Then the computational model including ECM stiffness is calibrated to experimental results in section 3.1. This is followed by the sections 3.2-3.5, where each section treats one of the four research objectives mentioned above. The findings are discussed in section 4, accompanied by suggestions for future research directions.

2

Material and Methods

In this thesis, the regulation of tip/stalk cell patterning is investigated using a computational model in C++. The signaling pathways within an endothelial cell are described by a mathematical model [24], which in this study is extended to include mechanical influences from ECM stiffness, as described in section 2.1. In section 2.2, endothelial cells are coupled together to simulate a vessel sprout under stimulus of a VEGF gradient field. This section also entails the computational setup for the model calibration to experimental data and for the studies conducted that address the research questions. All figures in the results section have been generated using Matlab software.

2.1. Modeling intracellular signaling for each cell

In a mathematical model, the intracellular concentrations of the proteins involved in the VEGF-induced Notch signaling pathway responsible for tip/stalk cell patterning are tracked. Using a system of coupled differential equations, the interactions between the proteins are described per cell (Eq. (2.1)-(2.8)). All function terms and corresponding parameters in Table 2.1 are corresponding to the mathematical model by Venkatraman et al. [24], except for the newly introduced stiffness-dependent functions ($S_1(k)$, $S_2(k)$).

Dll4 (D) and the Notch receptor (N) on a neighbouring cell can bind to each other and dissociate from one another. This is described with function terms $S_1(k)D{\cdot}N_{nb}$ and $k_{-2}\bar{N}_{nb}$ in Eq. (2.1), (2.2), (2.3), where the binding rate is the stiffness-dependent function S_1 (2.9). Once the Notch receptor is bounded ($\bar{N}$), several cleavage events follow that cause the release of the Notch intracellular domain (I), given by $k_4\bar{N}$ in Eq. (2.4). The Notch intracellular domain translocates to the cell nucleus, which leads to the upregulation of the HE genes (H). This is described through a Hill function with Hill coefficient n and half-maximal activation constant κ, given by $\theta\frac{I^n}{\kappa^n+I^n}$ in Eq. (2.7). Parameter κ represents the concentration of NICD at which the upregulation of HE is half-maximal. These HE genes inhibit the expression of VEGFR2 (R), by $k_3R\cdot H^n$ in Eq. (2.5). VEGF receptors can bind with VEGF and dissociate too. This is described with function terms $k_1V_s\cdot R$ and $k_{-1}\bar{R}$ in Eq. (2.5), (2.6), where V_s is the amount of VEGF sensed by filopodia (2.14). The bounded VEGF receptor ($\bar{R}$) stimulates filopodia (f) formation and upregulates the expression of Dll4, which is described with $k_5\bar{R}^n$ in Eq. (2.8) and $\theta\frac{\bar{R}^n}{\kappa^n+\bar{R}^n}$ in Eq. (2.1), respectively. However, in stiffer matrices Dll4 expression is suppressed, which is function term $S_2(k)D$ in Eq. (2.1), where S_2 is a stiffness-dependent function given by (2.10). Moreover, Dll4 and HE have a basal expression rate β. Notch, VEGFR2 and filopodia a basal production rate of γ. All proteins

undergo degradation with degradation rate ϕ and filopodia degrade with rate ϕ_f.

$$\frac{dD}{dt} = \beta - \phi D - S_1(k)D \cdot N_{nb} + k_{-2}\bar{N}_{nb} + \theta\frac{\bar{R}^n}{\kappa^n + \bar{R}^n} - S_2(k)D, \tag{2.1}$$

$$\frac{dN}{dt} = \gamma - \phi N - S_1(k)D_{nb} \cdot N + k_{-2}\bar{N}, \tag{2.2}$$

$$\frac{d\bar{N}}{dt} = - \phi \bar{N} + S_1(k)D_{nb} \cdot N - k_{-2}\bar{N}, \tag{2.3}$$

$$\frac{dI}{dt} = - \phi I + k_4\bar{N}, \tag{2.4}$$

$$\frac{dR}{dt} = \gamma - \phi R - k_1 V_s \cdot R + k_{-1}\bar{R} - k_3 R \cdot H^n, \tag{2.5}$$

$$\frac{d\bar{R}}{dt} = - \phi \bar{R} + k_1 V_s \cdot R - k_{-1}\bar{R}, \tag{2.6}$$

$$\frac{dH}{dt} = \beta - \phi H + \theta\frac{I^n}{\kappa^n + I^n}, \tag{2.7}$$

$$\frac{df}{dt} = \gamma - \phi_f f + k_5\bar{R}^n, \tag{2.8}$$

Parameter	Value	Unit	Explanation
k_1	0.1	$(c \cdot s)^{-1}$	VEGF-VEGFR2 binding rate
k_{-1}	0.001	s^{-1}	VEGF-VEGFR2 dissociation
k_2	0.001	$(c \cdot s)^{-1}$	Dll4-Notch binding rate at 1 kPa
k_{-2}	0.1	s^{-1}	Dll4-Notch dissociation
k_3	0.005	$c^{-n} \cdot s^{-1}$	VEGFR2 inhibition by HE
k_4	0.1	s^{-1}	Dll4-Notch cleavage
k_5	0.1	$c^{1-n} \cdot s^{-1}$	Filopodia induction by bounded VEGFR2
β	0.001	$c \cdot s^{-1}$	Basal gene expression
γ	0.005	$c \cdot s^{-1}$	Receptor production
ϕ	0.005	s^{-1}	Protein degradation
θ	0.1	$c \cdot s^{-1}$	Upregulation rate
ϕ_f	0.001	s^{-1}	Filopodia degradation
n	2	dimensionless	Hill coefficient
κ	1	c	Half-maximal activation constant

Table 2.1: Parameters corresponding to the system of ODEs. Concentrations are expressed in concentration units c. Time is in seconds s.

The influence of ECM stiffness on the Notch pathway is included through YAP-mediated Dll4 suppression [17]. This is done through a Hill function

$$S_1(k) = c_1\Big(\frac{k-1}{c_2 + k - 1}\Big), \tag{2.9}$$

where k is the ECM stiffness. The function is shifted to assume no Dll4 inhibition at a stiffness of 1 kPa. This is the reference value to which the multiple stiffness levels are calibrated against the experimental data.

Secondly, the influence of ECM stiffness is included through a decrease in Notch binding [15]. This is done through a suppressive Hill function

$$S_2(k) = k_2\Big(\frac{c_3}{c_3 + (k-1)^{n_2}}\Big), \tag{2.10}$$

where the function is shifted so that at a stiffness of 1 kPa, the Notch binding rate is assumed to be equal to k_2. The choice of these functions and parameters will be further explained in section 2.2.1.

2.2. Modeling a vessel sprout under VEGF stimulation

In order to study the tip/stalk cell patterning, a row of endothelial cells of $10\ \mu m \times 10\ \mu m$ [3] is simulated, representing a micro vessel in early sprouting angiogenesis (Fig. 2.1). The vessel sprout is assumed to be 10 cells long, to satisfy the minimum length for branching [22].

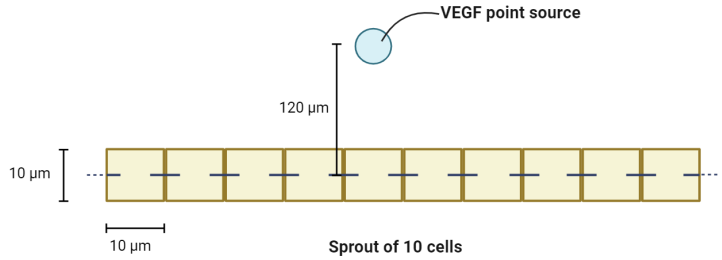

Figure 2.1: Visual representation of the vessel sprout relative to the VEGF point source.

Each individual cell contains the mathematical model describing the Notch signaling pathway discussed in the previous section. Between neighbouring cells, Dll4 can bind to the Notch receptor. The outer most left cell is considered a neighbour to the outer most right cell, to avoid unwanted boundary effects. The cells are initialized such that they are all stalk cells (low filopodia) with values [24]

$$\{D = 0, \quad N = 1, \quad \bar{N} = 0, \quad I = 0, \quad R = 1, \quad \bar{R} = 0, \quad H = 0, \quad f = 0\}.$$

The vessel sprout is stimulated by a VEGF gradient field modeled by

$$\frac{\partial V_a(\mathbf{x},t)}{\partial t} = d\Delta V_a - k_{deg} V_a + V_{in} 1_{\mathbf{x}=(x_p,y_p)}, \qquad \mathbf{x} \in \Omega, \tag{2.11}$$

$$V_a(\mathbf{x},t) = 0, \qquad \mathbf{x} \in \delta\Omega, \tag{2.12}$$

$$V_a(\mathbf{x},0) = 0, \qquad \mathbf{x} \in \Omega \cup \delta\Omega, \tag{2.13}$$

where Ω is the square of $0 < x < 1010\ \mu m$ and $0 < y < 1010\ \mu m$. Dirichlet boundary conditions make sure the VEGFs can exit freely out of the region. d represents the diffusion rate, k_{deg} the degradation rate and the last term models a point source with an influx strength of V_{in}. This source is placed at $\mathbf{x} = (x_p, y_p)$, where (x_p, y_p) is the point in the middle of the Ω square, 120 microns above the fifth cell in the vessel sprout. This distance is chosen such that the amount of VEGF arriving at the cells is similar to the input of the model of Venkatraman et al. [24]. The VEGF field parameters are given by $d = 10\ \mu m s^{-1}$, $k_{deg} = 1.6 * 10^{-4}\ s^{-1}$, $V_{in} = 0.5\ c$ [20]. The VEGF gradient field is discretized using a central difference scheme with a spatial step of 10 microns.

After initialization, the model will do an update with a time step of 1 second. Firstly, the available VEGF at each place in the field is derived using Forward Euler time integration. The stability of this time integration method is determined in Appendix A. Secondly, by iterating over all cells in the vessel sprout, Forward Euler time integration over the system of differential equations in the previous section is used to calculate the protein concentrations within a cell. These two steps are done separately, since for each individual cell a set of equations is solved.

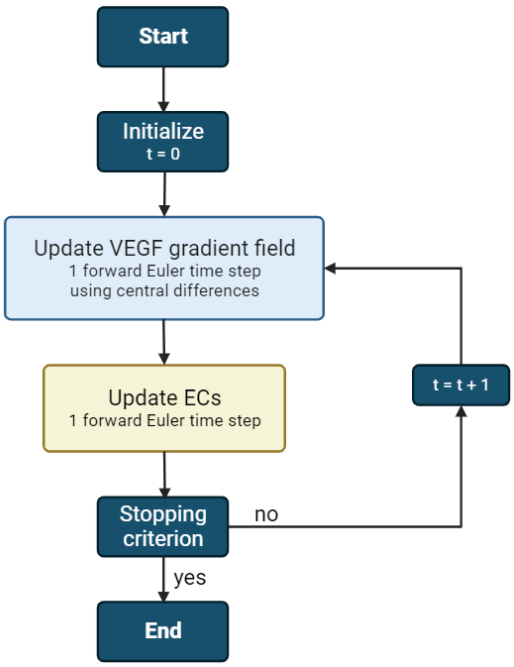

Figure 2.2: Flowchart of the computational model simulations.

The input for this set of ODEs is the VEGF sensed by filopodia (V_s), which is captured by the following equation:

$$V_s = V_a(2s(f) - 1), \tag{2.14}$$

where $s(f)$ is the sigmoid function

$$s(f) = \frac{1}{1 + e^{-af}}. \tag{2.15}$$

By using this function, a cell with a high concentration of filopodia can sense many more growth factors than a cell with a lower concentration. The size of this difference is determined by the parameter a and is taken to be $a = 0.06$. Other choices for this parameter are investigated in section 3.3. Another input to the set of equations is the Dll4 and Notch concentrations from neighbouring cells. These values are taken from the previous time step to avoid a time bias from left to right.

After the iteration process over all cells is complete, the update of 1 second is done. These updates repeat themselves until a stopping criterion is met. In all studies, the computational model is stopped either after a specific time point, or when a possible steady state solution is found. This is done with the following stopping criterion, which checks if the filopodia has changed in the last two hours.

$$\forall n \in \{1, \ldots, 10\}: \quad |f_n(t) - f_n(t - 2 \text{ hours})| < \epsilon, \tag{2.16}$$

where $f_n(i)$ represents the filopodia concentration of cell n out of 10 cells at time t and ϵ is given by $\epsilon = 10^{-3}\ c$. A change in solution is not expected after this criterion is met, since the cells receive no new stimuli. A schematic of the whole process is shown in figure 2.2.

2.2.1. Model calibration to ECM stiffness

The stiffness-dependent functions S_1 and S_2 (Eq. 2.9, 2.10) are calibrated to match the *in vitro* experiment by Matsuo et al. [17]. In this experiment, the protein expression in HUVECs, a type of endothelial cells often used in experiments to study angiogenesis, is measured in a gel-environment of 1, 2, 4, 8 and 25 kPa to simulate a weak to stiff substrate, after being stimulated by VEGFs (Fig. 2.3).

The model parameters from Venkatraman et. al. [24] are assumed to be the reference model at 1 kPa. Parameters from the newly introduced stiffness-dependent functions, S_1 and S_2 are found by calibrating through trial and error to the total Dll4 and NICD concentrations, and then compared to the total Notch concentration. The predicted total protein concentration is defined as the predicted concentration of a specific protein summed over all cells, in the predicted steady state. The obtained parameters are given by

$$\{c_1 = 0.084, \quad c_2 = 52, \quad c_3 = 120, \quad n_2 = 1.84\}.$$

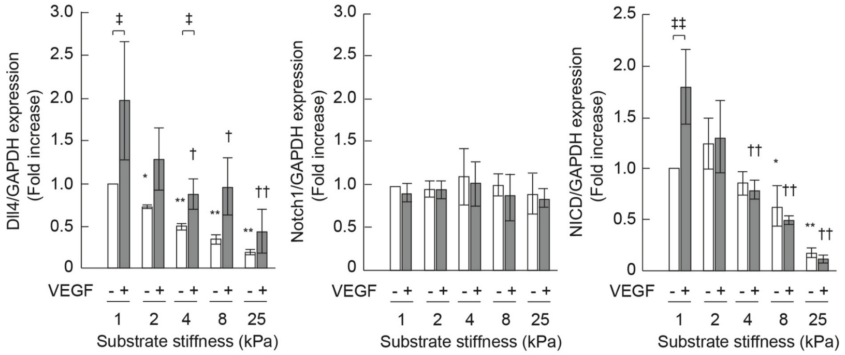

Figure 2.3: Experimental measurements of Dll4, Notch and NICD concentrations (fold increase) in different stiffness environments, with and without VEGF stimulation [17].

The calibration results are quantified by taking the average of the mean absolute error (MAE) over Dll4 and NICD:

$$\text{Average MAE} = \frac{1}{2}\Big(\frac{1}{4}\sum_{k=\{2,4,8,25\}} |\mathbf{D}_k - \hat{\mathbf{D}}_k| + \frac{1}{4}\sum_{k=\{2,4,8,25\}} |\mathbf{I}_k - \hat{\mathbf{I}}_k|\Big), \tag{2.17}$$

where $\hat{\mathbf{D}}_k$ and $\hat{\mathbf{I}}_k$ are the model predicted protein concentrations of the 10 cells combined of Dll4 and NICD, respectively, and $\mathbf{D}_k$ and $\mathbf{I}_k$ are the experimental observations, all relative to 1 kPa.

2.2.2. The effect of ECM stiffness on tip/stalk cell patterning

To investigate how tip/stalk cell patterning is affected by ECM stiffness, filopodia concentrations in the vessel sprout are measured over stiffness levels ranging from 1 to 20 kPa, with intervals of 1 kPa. Complementing the filopodia predictions, an analysis of other key protein concentrations, including Dll4, bounded Notch, and VEGFR2, was conducted. This analysis aims for a better understanding of the signaling pathways responsible for tip/stalk cell patterning in angiogenesis.

2.2.3. Filopodia-mediated VEGF sensation

The degree to which filopodia can sense growth factors is hard to quantify. This study investigates different relations between filopodia concentration and their VEGF sensing ability across multiple stiffness values. In function (2.14), describing the filopodia-mediated VEGF sensation, parameter a is modulated to gain understanding of its influence on predicted cell patterning. The patterning behaviour at time points

$$\{t = 1, \quad t = 1.5, \quad t = 2, \quad t = 2.5\},$$

and at the steady state is predicted for different values of parameter a

$$\{a = 0.01, \quad a = 0.02, \quad a = 0.06, \quad a = 0.1, \quad a = 0.15\},$$

in a stiffness range of 1 to 20 kPa.

2.2.4. Modulating VEGF binding for angiogenic treatments

To investigate how an increase and decrease of the VEGF binding affect the tip/stalk cell patterning, the model was run for different values of the parameter k_1, representing the VEGF binding rate

$$\{k_1 = 0.015, \quad k_1 = 0.025, \quad k_1 = 0.1, \quad k_1 = 0.4\}.$$

This was performed at two time points, 1.5 and 5 hours, and until the steady state solution. The model was run for stiffness values ranging from 1 to 20 kPa.

2.2.5. The influence of bounded Notch cleavage

The current model accounts for the release of NICD as a result of the binding of the Notch receptor. However, the cleavage of the bounded Notch receptor is not included. Hence, for this study, the model is adjusted to incorporate this cleavage event that results in the release NICD. Equation (2.3), describing the concentration of bounded Notch, is altered to

$$\frac{d\bar{N}}{dt} = -\phi\bar{N} + S_1(k)D_{nb} \cdot N - k_{-2}\bar{N} - k_4\bar{N}, \tag{2.18}$$

where the last term represents the bounded Notch cleavage.

Parameter θ, the upregulation rate, is split up into θ_1, responsible for Dll4 upregulation through VEGF binding, and θ_2, responsible for HE upregulation through NICD nuclearization, to indicate two different processes. Parameters θ_1, θ_2, and parameters governing the stiffness-dependent functions (2.9) and (2.10), are searched by trial and error to match experimental data by Matsuo et al. [17], to which the model excluding Notch cleavage is calibrated as well. Calibration results are again assessed using the averaged MAE score. The obtained parameters are given by

$$\{\theta_1 = 0.2, \quad \theta_2 = 0.15, \quad c_1 = 0.12, \quad c_2 = 52, \quad c_3 = 1.26, \quad n_2 = 0.92\}.$$

The cell patterning is predicted for multiple choices of θ_1 and θ_2, to highlight their influence on the cell patterning over various ECM stiffness levels.

The steady state cell patterning, and the cell patterning after 1.5 hours is predicted, allowing for a comparison between the two models. This is done for an ECM stiffness of 1 to 7 kPa, with intervals of 0.33 kPa. The VEGF binding rate is modulated as well, allowing for the investigation of the influence of the Notch cleavage on cell patterning, depending on this binding rate.

3

Results

3.1. Model calibration to ECM stiffness

In figure 3.1, the total protein concentration of Dll4 and NICD, relative to 1 kPa, are depicted for varying ECM stiffness levels. The model's predictions, represented by the blue lines, indicate a reduction in both Dll4 and NICD concentration with increasing ECM stiffness. Notably, a temporary rise in concentration is observed within the stiffness range of 14 and 16 kPa, corresponding to the patterning failure (Fig. 3.4a, section 3.2). Generally, the model's predictions closely align with the experimental data (depicted by orange), with the exception of the 8 kPa stiffness level. The averaged MAE score is 0.054.

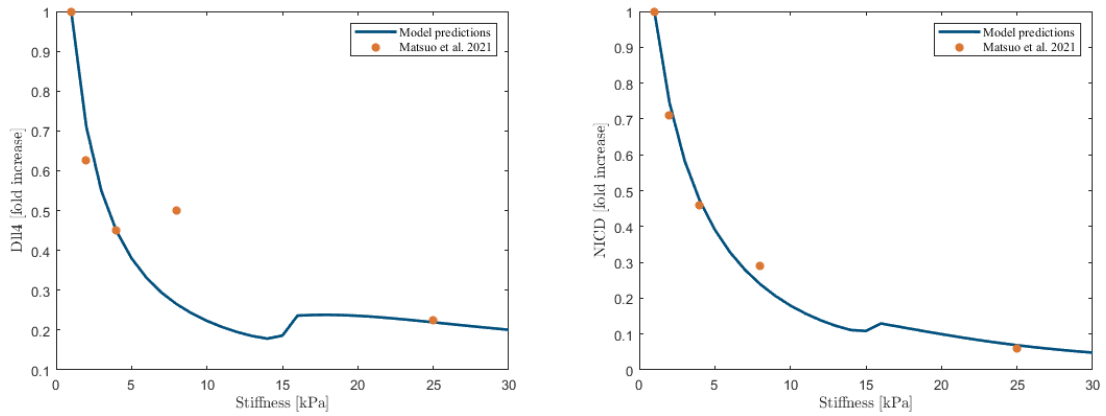

Figure 3.1: Protein concentration of 10 cells combined (fold increase). The orange dots are the findings of the *in vitro* experiment [17]. The blue lines represent the computational model predictions. (a) Dll4 concentration (b) NICD concentration

The calibrated model is compared to the Notch measurements (Fig. 3.2). The relative change in total Notch concentration when varying ECM stiffness is relatively small, both experimentally and in the model predictions. A small increase in Notch concentration is predicted with increasing ECM stiffness, while experimentally, for higher stiffness values, a decrease in Notch concentration was determined.

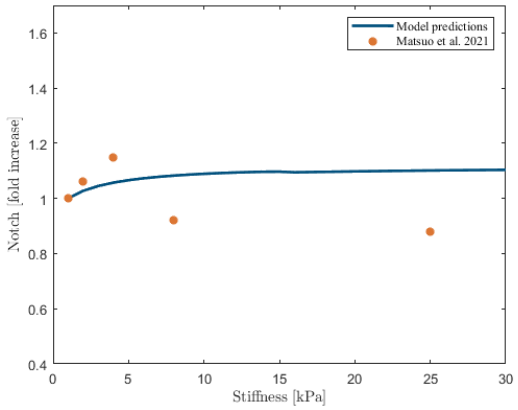

Figure 3.2: Notch concentration of 10 cells combined. The orange dots are the findings of the *in vitro* experiment [17]. The blue lines represent the computational model predictions.

3.2. The effect of ECM stiffness on tip/stalk cell patterning

In this study, the influence of ECM stiffness on cell patterning is investigated, specifically focusing on its influence on the key proteins involved in the VEGF-induced Notch signaling pathway.

The model predicts a steady state solution of a salt-and-pepper pattern of alternating tip and stalk cells for an ECM stiffness of 1 kPa (Fig. 3.3). The tip cells are characterized by a high filopodia concentration (green), whereas the stalk cells have a low filopodia concentration (yellow).

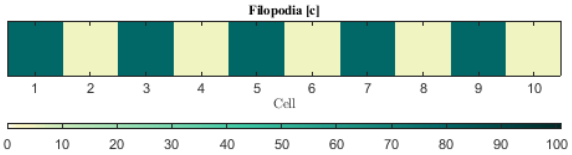

Figure 3.3: Model prediction of the cell pattern in terms of filopodia concentration at an ECM stiffness of 1 kPa.

Upon increasing ECM stiffness, the model continues to predict a salt-and-pepper pattern as the steady state solution (Fig. 3.4a). However, beyond a stiffness threshold of 15 kPa, no patterning is observed at all, and all cells exhibit a moderately high filopodia concentration. Figure 3.4b shows the filopodia patterning at an earlier time point of 1.5 hours. For ECM stiffness values below 3 kPa and above 10 kPa, the patterning is less apparent. Hence, the emergence of opposite cell states occurs at a comparatively slower pace in these stiffness ranges.

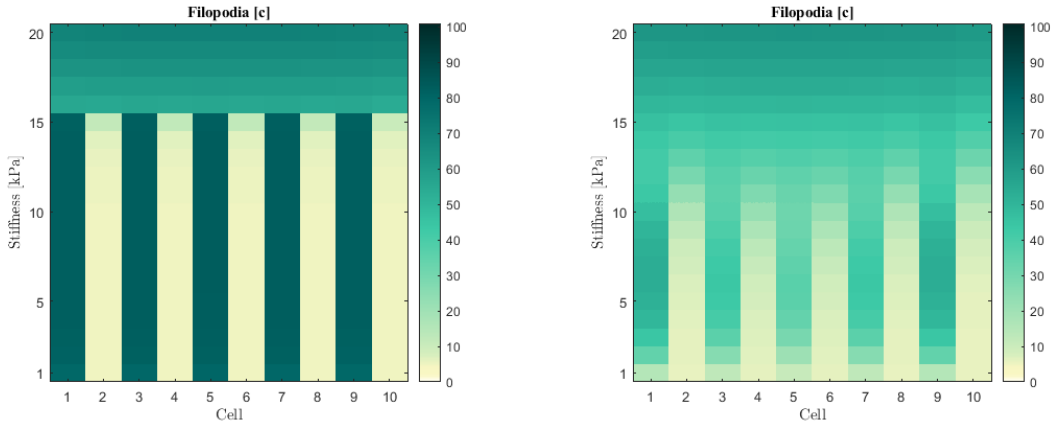

Figure 3.4: Model predictions of the cell pattern in terms of filopodia concentration over ECM stiffness values from 1 to 20 kPa (y-axis). (a) Steady state solution (b) After 1.5 hours

The computer model predicts that a small change in ECM stiffness can lead to a pattern failure. At 15 kPa the cells still alternate between a high and low filopodia concentration, whereas at 16 kPa this alternation is not observed anymore. VEGF-induced Notch signaling makes sure small differences are enhanced and result in opposite cell states. However, when Notch signaling is damped, these small differences between cells, like VEGF uptake, remain small. A clearer understanding of how this is accomplished can be gained through an examination of the patterning of other associated proteins at a steady state solution (Fig. 3.5).

A rise in stiffness results in a decrease of Dll4, especially in the tip cells (Fig. 3.5a). This leads to a decrease in Notch binding, particularly in stalk cells (Fig. 3.5b). This lack of Notch communication between cells causes a reduction of VEGFR2 inhibition in stalk cells (Fig. 3.5c), which is important for the creation of the opposite cell states, tip and stalk. The model predicts that for a too high ECM stiffness, 16 kPa in the numerical simulation, this lack of inhibition results in the failing of cell patterning.

The slow filopodia patterning under 3 kPa, observed in figure 3.4b, can be linked to the presence of Notch binding in tip cells seen in figure 3.5a. This results in mutual lateral inhibition, slowing down the emergence of opposite cell states.

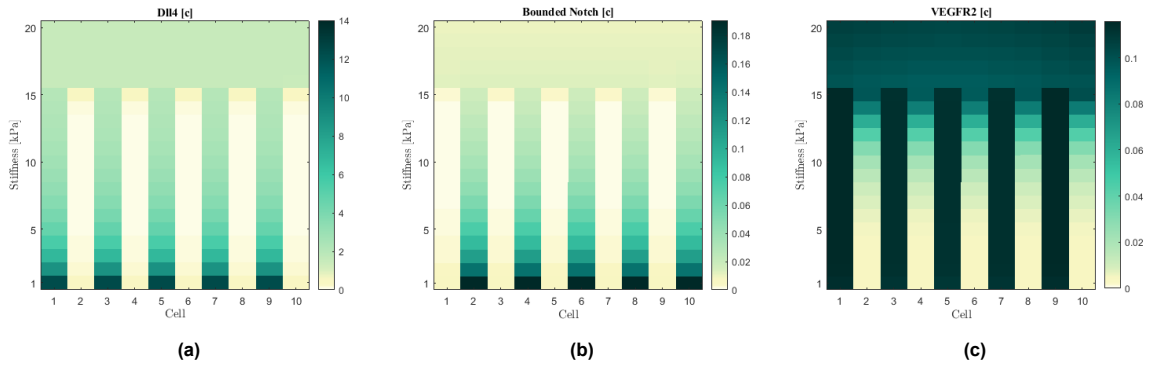

Figure 3.5: Model predictions of the cell pattern of over ECM stiffness values from 1 to 20 kPa at a steady state solution. (a) Dll4 concentration (b) Bounded Notch concentration (c) VEGFR2 concentration

3.3. Filopodia-mediated VEGF sensation

In this section, the choice of parameter a in equation (2.14), responsible for filopodia-dependent VEGF sensation, is investigated based on its effect on the cell patterning. Parameter a determines the sensitivity of VEGF sensation to changes in filopodia concentration in a cell (Fig. 3.6). The dotted line represents the available VEGF concentration to the cell, based on its position in the gradient field. The colored lines depict how much of this available VEGF can be sensed, depending on the filopodia

concentration level.

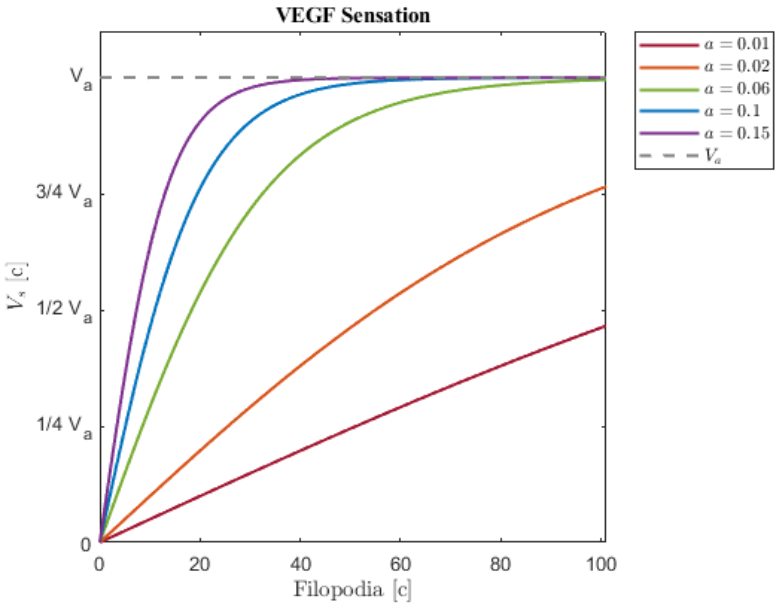

Figure 3.6: VEGF sensation of a cell for various values of a, captured by equation (2.14).

Figure 3.7 shows the cell patterning for various values of a at different time points. According to the model predictions, higher values of a result in faster patterning. This phenomenon can be explained by the observation that for a higher value of a, a minor rise in filopodia leads to relatively more VEGF uptake, as compared to a lower value of a, causing opposite cell states to emerge sooner. Although, in the steady state is predicted that higher values of a experience pattern failure in a lower level of ECM stiffness.

When a is too high ($a = 0.15$, Fig. 3.8), the cells exhibiting a low filopodia concentration sense a relatively high level of VEGF. Consequently, they induce lateral inhibition towards their neighbours too, dampening the difference between the opposite cell states. Moreover, the model predicts that the emergence of the salt-and-pepper pattern is slowed down for this excessive value of a. When a is too low ($a = 0.01$, Fig. 3.8), no patterning is observed due to the lack of filopodia formation.

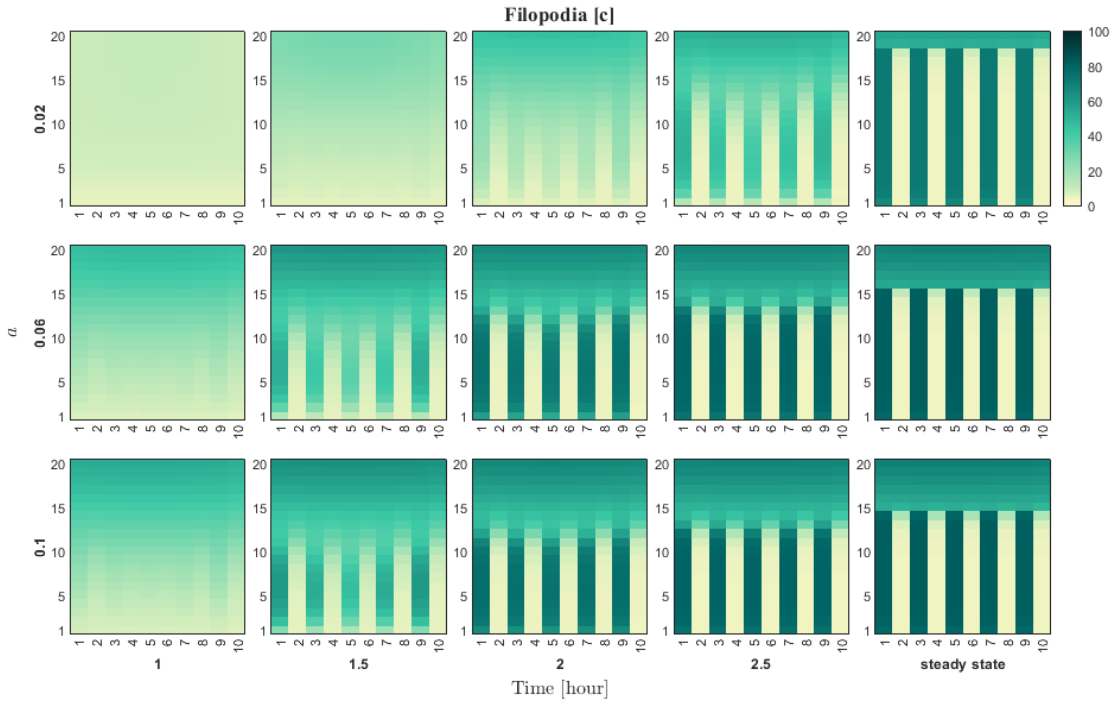

Figure 3.7: Model predictions of the cell pattern in terms of filopodia concentration at an ECM stiffness of 1 to 20 kPa. This is done for various choices of a (y-axis) and time points (x-axis).

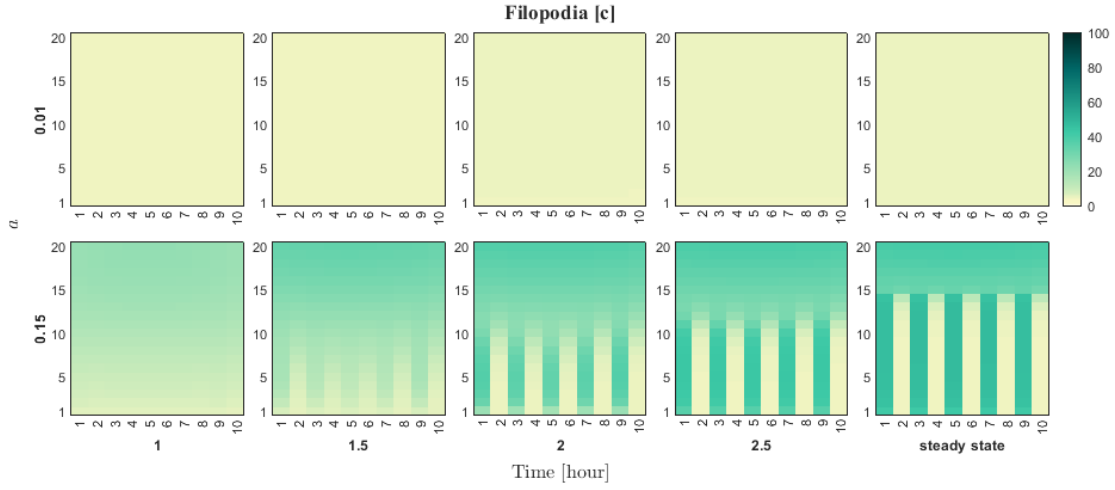

Figure 3.8: Model predictions of the cell pattern in terms of filopodia concentration at an ECM stiffness of 1 to 20 kPa. This is done for an excessively low $a = 0.01$ and high $a = 0.15$ parameter choice (y-axis) and at various time points (x-axis).

3.4. Modulating VEGF binding for angiogenic treatments

In this section, the cell pattern is studied for various VEGF binding rates (Fig. 3.9). The model predictions show that a low binding rate ($k_1 = 0.025$) results in weak opposite cell states, while a high binding rate ($k_1 = 0.4$) achieves strong opposite cell states, characterized by tip cells exhibiting a high concentration of filopodia. Moreover, at a high VEGF binding rate these opposing cell states emerge faster.

However, the elevated VEGF binding also results in a failure of patterning under lower stiffness conditions, as compared to simulations with a low binding rate. An excessively low binding rate ($k_1 = 0.015$) yields insufficient lateral inhibition, resulting in pattern failure at lower stiffness conditions as well.

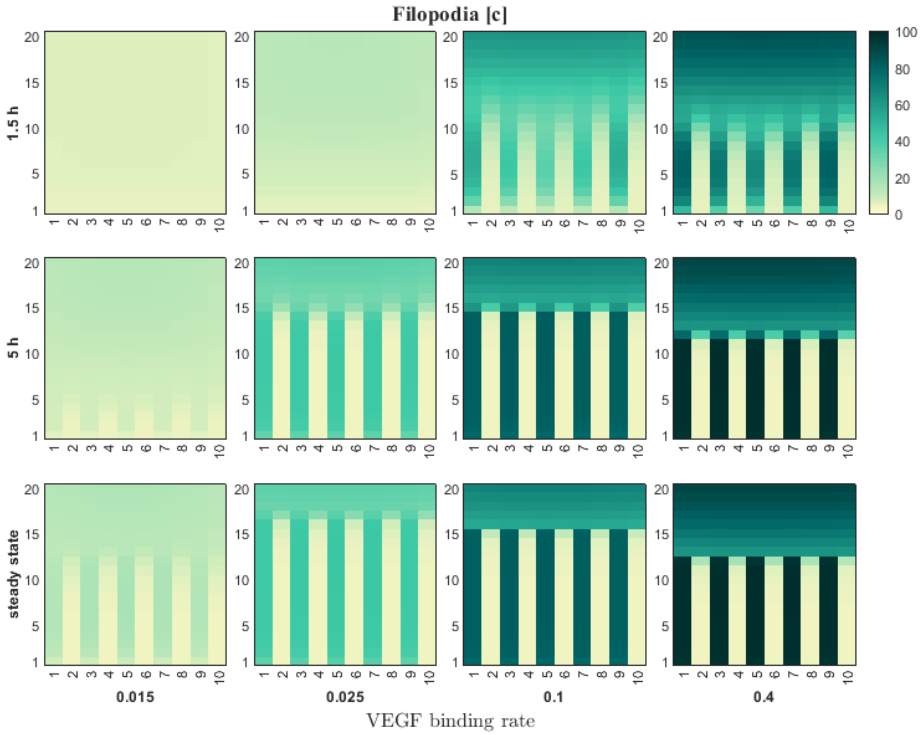

Figure 3.9: Cell pattern of the vessel sprout in terms of filopodia concentration at an ECM stiffness of 1 to 20 kPa. This is done for various VEGF binding rates (y-axis) and time points (x-axis).

3.5. The influence of bounded Notch cleavage

3.5.1. Model calibration

Figure 3.10 shows the calibration results of the model including Notch cleavage. The peak in protein concentrations, indicative of the abrupt transition from pattern success to failure, occurs now at a lower stiffness value (4.67-5 kPa), compared to the model excluding Notch cleavage. This shift is noteworthy as it allows the model predictions to align more accurately with a stiffness of 8 kPa, which was not the case in the previous model. The averaged MAE score is 0.021.

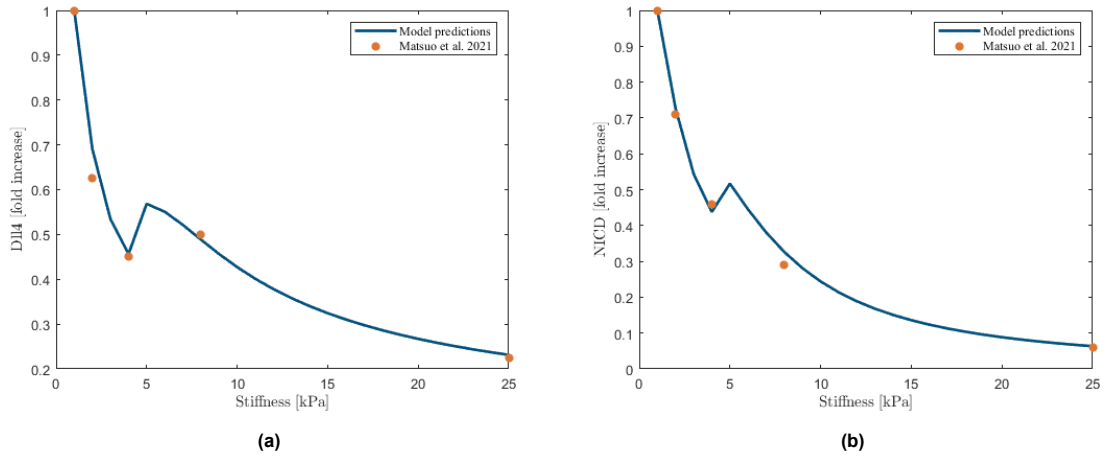

Figure 3.10: Protein concentration of 10 cells combined (fold increase). The orange dots are the findings of the *in vitro* experiment [17]. The blue lines represent the computational model predictions, including the cleavage of bounded Notch. (a) Dll4 concentration (b) NICD concentration.

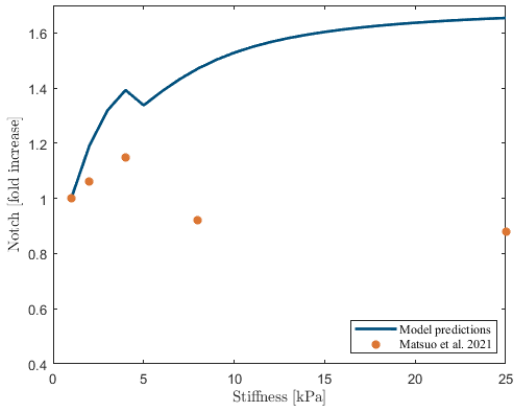

Figure 3.11: Notch concentration of 10 cells combined. The orange dots are the findings of the *in vitro* experiment [17]. The blue lines represent the computational model predictions, including the cleavage of bounded Notch.

Despite the improvements in calibration, the model still faces difficulties in accurately predicting the total Notch concentration. Nevertheless, in accordance with the experimental findings, a decrease in concentration is observed following the peak at 4 kPa. However, the model's predicted decrease is relatively minor compared to the experimental measurements.

3.5.2. The influence of bounded Notch cleavage on cell patterning

The computer model predicts that the salt-and-pepper pattern failure occurs at 4.67 kPa (Fig. 3.12b). This threshold is three times lower than that observed in the model excluding Notch cleavage (Fig. 3.12a). The moment of pattern failure is highly dependent on the choice of parameter θ_1 and θ_2 (Appendix B). The model predicts that higher values for these parameters result in the formation of cell patterning at increased levels of stiffness.

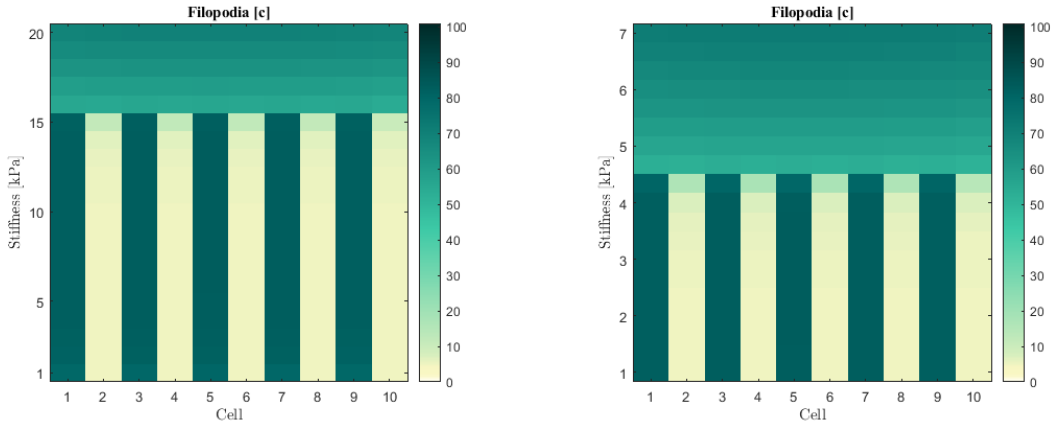

Figure 3.12: Model predictions of the cell pattern in terms of filopodia concentration over various ECM stiffness values at a steady state solution. (a) Excluding Notch cleavage (b) Including Notch cleavage

A comparison of the predictions at a time point of 1.5 hours reveals that the inclusion of Notch cleavage accelerates the formation of patterning at low ECM stiffness levels (Fig. 3.13a).

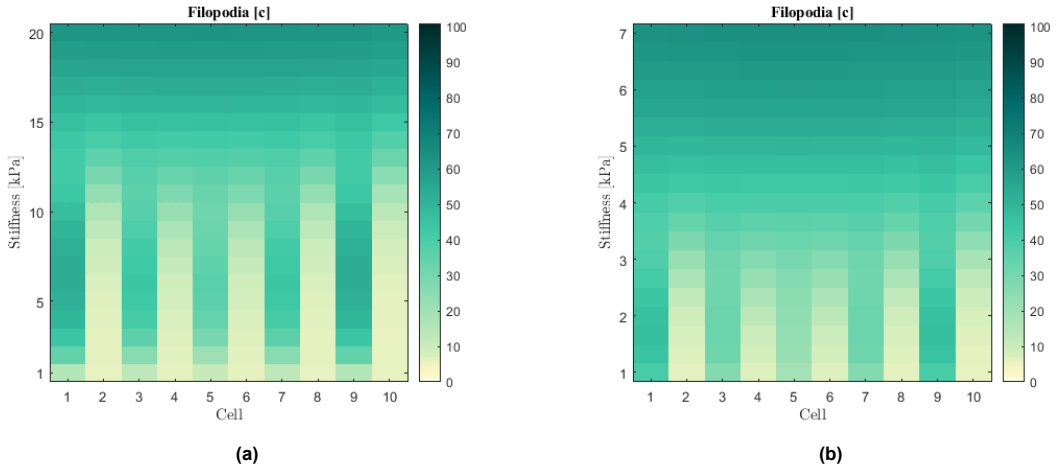

Figure 3.13: Model predictions of the cell pattern in terms of filopodia concentration over various ECM stiffness values at 1.5 hours. (a) Excluding Notch cleavage (b) Including Notch cleavage

To further investigate the influence of bounded Notch cleavage on cell patterning, the steady state pattern for multiple VEGF binding rates iss predicted (Fig. 3.14). Table 3.1 denotes the stiffness levels k at which pattern failure is predicted by the two different models. The Pattern Failure Stiffness ratio (PFS), which is the pattern failure stiffness of the model excluding Notch cleavage, divided by that of the model including Notch cleavage, is calculated to quantify the difference in the two models related to the VEGF binding rate. The PFS ratio increases with the VEGF binding rate, indicating that the stiffness threshold for which patterning fails, is relatively lower for the model including Notch cleavage. Hence, for higher binding rates, this model shows a higher sensitivity for pattern failure.

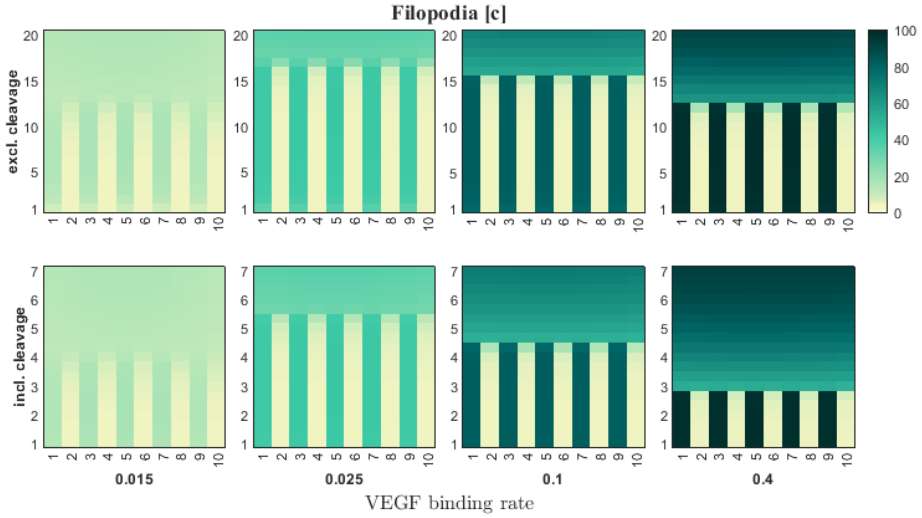

Figure 3.14: Model predictions of the cell pattern in terms of filopodia concentration for various ECM stiffness values. This is done for various VEGF binding rates (x-axis), by the model excluding and including bounded Notch cleavage (y-axis).

Binding rate k_1	0.015	0.025	0.1	0.4
Stiffness k for which pattern fails (excl. cleavage)	13	18	16	13
Stiffness k for which pattern fails (incl. cleavage)	4.33	5.67	4.67	3
PFS ratio	3	3.17	3.43	4.33

Table 3.1: Stiffness value k [kPa] for which patterning fails. The predictions for the model, excluding and including bounded Notch cleavage. The PFS ratio denotes the ratio of pattern failure stiffness.

4

Discussion

In this thesis, a computational model is created that allows for investigation of the intricate dynamics of tip/stalk cell patterning in early sprouting angiogenesis, focusing specifically on how it is affected by the extracellular matrix stiffness.
Changes in protein concentrations associated with signaling pathways involved and their response to varying ECM stiffness are investigated, offering valuable insights into the predicted cell patterning outcomes.
In the computational model, a dynamic VEGF field is modeled to simulate a realistic setting. A study is conducted that explores multiple relationships to capture filopodia-mediated VEGF sensation.
Furthermore, the VEGF binding rate is modulated to gain more insight on how ECM stiffness impacts angiogenic treatments-based on VEGF binding.
Lastly, the model is further developed to include the cleavage of the bounded Notch receptor, aiming to investigate its influence on cell patterning through various stiffness levels.
In this section, the conclusions drawn from the respective studies will be examined and discussed.

4.1. Model calibration to ECM stiffness

The model parameters of the Venkatraman model are assumed to correspond to an extracellular matrix stiffness of 1 kPa. Taking this as a reference value, the model is calibrated to fit to the experimental data over various stiffness levels by only adjusting the stiffness-dependent functions. The computer model is able to align its predictions to the Dll4 and NICD concentrations well, except at an ECM stiffness of 8 kPa. Conversely, the decrease in Notch concentration for higher stiffness values observed in the experiment, is not predicted by the computer model. Improving the alignment of the model predictions with the experimental data requires further examination of the connections between ECM stiffness and the Notch signaling pathway.

The misalignment could also be a consequence of differences between the experimental and computational setup. In the computational model, the VEGF gradient field is simulated with a constant influx and permits diffusion out of the region of interest, which contrasts with the experimental conditions. Additionally, the row of ten aligned endothelial cells in the computational setup may not accurately reflect the confluent HUVECs in the cell culture dishes. These variations could potentially account for the observed differences in Notch concentration.

Given that the experimental data used for calibration are measurements relative to 1 kPa, a deviation in the parameter set assumed to correspond to this value would induce a shift in stiffness within the model predictions. Therefore, in the current model, it is advisable to interpret the predictions in a relative sense.

4.2. The effect of ECM stiffness on tip/stalk cell patterning

Kretschmer et al. found that a rise in stiffness enhances network formation, but a too stiff ECM can impede the process [14]. Additionally, Bentley et al. states that a faster patterning time results in denser networks [2]. The model's predictions align with these findings: with a rise in ECM stiffness,

opposite cell states emerge more rapidly, which according to Bentley. et. al. results in a denser network. However, in an ECM that is too stiff, the patterning time slows down, resulting in a sparser network. It should be noted that the model lacks calibration to time. Nevertheless, the conclusion remains valid, as it is drawn in a relative context.

After a certain stiffness threshold, the model predicts pattern failure in which all cells exhibit a moderately high filopodia formation. It's crucial to clarify that this does not necessarily mean that all cells are tip cells ready for sprouting. Firstly, in this thesis, the criterion for defining a tip cell is assumed to be a high filopodia level. However, diverse conditions have been used in previous computer models to classify a cell as tip cell, such as a threshold for Dll4 or NICD concentration [20, 19]. Secondly, it might become mechanically more challenging for a tip cell to initiate sprouting if every cell attempts to pull itself forward.

4.3. Filopodia-mediated VEGF sensation

The ability of filopodia to sense VEGFs is case-specific as it varies depending on various factors. ECM properties, including stiffness, as well as factors such as filopodia length and the distribution of VEGFR receptors, can influence their sensing ability. Considering these aspects, a spectrum of function choices of filopodia-mediated VEGF sensation are considered based on parameter a, exhibiting variations in the sensitivity of VEGF sensation to an increase in filopodia concentration. A high value of a corresponds to a higher rise in VEGF sensation for an increase in filopodia concentration, as compared to a low value of a.

Zakirov et al. [26] demonstrated through both *in silico* and *in vivo* experiments that a reduced probability of filopodia extension slows patterning down. This is in agreement with the outcomes observed in this study, where the model predicts that for a reduced ability of filopodia to sense VEGF, corresponding to a lower value of a, the patterning time increases.

Furthermore, the computer model predicts that a higher sensitivity in filopodia-mediated VEGF sensation leads to patterning failure in less stiff environments. To validate these predictions, additional experimental data based on various ECM stiffness levels is required.

4.4. Modulating VEGF binding for angiogenic treatments

The model predicts that a low VEGF binding rate leads to weak opposite cell states. Given that filopodia aid in cell migration, this observation could be an indication of fewer sprouts and consequently a sparser network. A decreased VEGF binding rate could therefore be advantageous for anti-angiogenic treatments. Conversely, simulations with a high VEGF binding rate lead to stronger opposite cell states. The tip cells exhibit a high filopodia concentration, possibly indicating increased sprout formation. This gives rise to a denser network, which is desired for an effective wound or bone healing process. This is in line with the *in vitro* and *in vivo* experiments by Hsieh et al., where elevated VEGFR2 internalization led to an increase in vessel branches [10].

However, the pattern failure predicted in lower stiffness conditions suggests that an increased binding rate is not always favourable. There is currently a lack of experimental data to confirm the predictions based on ECM stiffness. However, the model predictions show that a success or failure of the pattern varies significantly with ECM stiffness, indicating the importance of considering ECM stiffness in the exploration of angiogenic treatments based on VEGF binding.

4.5. The influence of bounded Notch cleavage

Literature sources, such as Kretschmer et al. [14] and Guo et al. [8], report varying stiffness levels for which network formation is prevented (e.g. 4 kPa or 15 kPa), dependent on the experimental setup. Hence, determining the accurate stiffness of pattern failure is challenging and situation dependent. However, the models in this thesis allow for the study of cell patterning in a relative sense.

The computational model including Notch cleavage predicts a pattern failure for ECM stiffness values lower than those predicted by the model without Notch cleavage. This prediction aligns with the expectation that the inclusion of Notch cleavage decreases Notch communication, thereby reducing lateral inhibition and therefore limiting pattern formation. This earlier failure of the pattern is able to explain the increase in Dll4 concentration for a matrix stiffness of 8 kPa observed experimentally. Overall, this model is able to achieve an improved alignment with the experimental data compared to the model

excluding cleavage, as it exhibits an averaged MAE score that is 2.5 times lower. However, the Notch concentration predictions do not show a significant improvement.

Furthermore, from the cell pattern predictions at 1.5 hours, it could be concluded that the model including Notch cleavage exhibits faster patterning in the low stiffness range. This behavior could be attributed to a reduction in Dll4, as an excess of Dll4 in all cells would increase the time needed for the establishment of opposing cell states.

Additionally, a comparison study of the two models is performed for various VEGF binding rates. The model including Notch cleavage predicts increased sensitivity of pattern failure to stiffness for higher VEGF binding rates. However, a confirmation of these predictions requires more experimental data.

Overall, the incorporation of bounded Notch cleavage exhibits a stiffness-dependent impact on cell patterning, emphasizing the importance of considering this factor in studies across varying cell stiffness environments. While the model demonstrates improved calibration to the experiment, further refinement through a parameter study is advised for a closer alignment to the experimental data.

4.6. Limitations and future work

In the current model, two ECM stiffness dependencies are incorporated: YAP-mediated Dll4 suppression and the decrease of Notch binding. Incorporating more relations between ECM stiffness and relevant proteins into the model has the potential to improve the models' accuracy. Existing literature suggests a connection between the mechanosensitive YAP protein and VEGFR2 [8, 25]. Moreover, in this study, the model predictions of Notch concentration do not align well with the experimental data, prompting an investigation into the relation between ECM stiffness and the Notch receptor.

To further develop the model, temporal calibration should be considered. This allows for time-specific predictions of the tip-cell selection, and consequently the time of sprouting.

For future studies on cell patterning dependent on ECM stiffness, it is advised to built upon the model including the cleavage of bounded Notch. The upregulation parameter θ is adjusted to fit the model to experimental data. However, a comprehensive investigation into alternative parameter combinations is suggested. This exploration will give insight on how varying parameters influence cell patterning at different ECM stiffness levels.

Furthermore, the VEGF gradient field could be adjusted to better replicate real-world conditions by including the VEGF uptake by filopodia. Moreover, filopodia-mediated VEGF sensation could be further developed to allow for sensation in surrounding grid points based on filopodia length.

Overall, the computer model developed in this thesis is able to predict tip/stalk cell patterning, marking the initial phase of sprouting angiogenesis. Following this event, tip cells migrate, and new sprouts emerge as a result of the elongation driven by the proliferation of follower stalk cells. To investigate the process of sprout formation and patterning, the model developed in this thesis could be coupled to a model dedicated to exploring sprout formation and patterning. Several models have been developed in the literature where sprout patterning is investigated using for example cell-based approaches [20, 4] or approaches based on agent-based modeling [16, 18]. The coupling of the model presented in this thesis with such models would enable the investigation of sprout patterning, where mechanical influences from ECM stiffness are included.

4.7. Conclusion

Existing models in the literature studying tip/stalk patterning during sprouting angiogenesis do not consider the influence of the extracellular matrix stiffness. The computational model presented in this thesis incorporates and emphasizes the impact of ECM stiffness, stressing its relevance in the investigation of angiogenic treatments. However, the validation and refinement of the model require additional experimental data. Further development of the model holds great promise for advancing our understanding of angiogenesis dynamics and contributing to more effective treatment strategies.

References

[1] *Angiogenesis - Wikipedia — en.wikipedia.org*. URL: https://en.wikipedia.org/wiki/Angiogenesis#/media/File:Angiogenesis_medical_animation_still.jpg.

[2] Katie Bentley, Holger Gerhardt, and Paul A Bates. "Agent-based simulation of notch-mediated tip cell selection in angiogenic sprout initialisation". In: *Journal of Theoretical Biology* 250 (1 2008), pp. 25–36. ISSN: 00225193. DOI: 10.1016/j.jtbi.2007.09.015. URL: www.elsevier.com/locate/yjtbi.

[3] Katie Bentley et al. "Tipping the balance: Robustness of tip cell selection, migration and fusion in angiogenesis". In: *PLoS Computational Biology* 5 (10 2009), p. 1000549. ISSN: 15537358. DOI: 10.1371/journal.pcbi.1000549. URL: www.ploscompbiol.org.

[4] Sonja E. M. Boas et al. *Cellular Potts Model: Applications to Vasculogenesis and Angiogenesis*. Springer, Cham, 2018, pp. 279–310. DOI: 10.1007/978-3-319-65558-1_18. URL: https://link-springer-com.tudelft.idm.oclc.org/chapter/10.1007/978-3-319-65558-1_18.

[5] J Dufraine, Y Funahashi, and J Kitajewski. "Notch signaling regulates tumor angiogenesis by diverse mechanisms". In: (). DOI: 10.1038/onc.2008.227. URL: www.nature.com/onc.

[6] Craig L. Duvall et al. "Impaired angiogenesis, early callus formation, and late stage remodeling in fracture healing of osteopontin-deficient mice". In: *Journal of Bone and Mineral Research* 22 (2 2007), pp. 286–297. ISSN: 08840431. DOI: 10.1359/jbmr.061103.

[7] Jennifer Flournoy, Shahad Ashkanani, and Yun Chen. *Mechanical regulation of signal transduction in angiogenesis*. Aug. 2022. DOI: 10.3389/fcell.2022.933474.

[8] Yaru Guo et al. "Matrix stiffness modulates tip cell formation through the p-PXN-Rac1-YAP signaling axis". In: *Bioactive Materials* 7 (May 2021 2022), pp. 364–376. ISSN: 2452199X. DOI: 10.1016/j.bioactmat.2021.05.033. URL: https://doi.org/10.1016/j.bioactmat.2021.05.033.

[9] M. R. Hausman, M. B. Schaffler, and R. J. Majeska. "Prevention of fracture healing in rats by an inhibitor of angiogenesis". In: *Bone* 29 (6 Dec. 2001), pp. 560–564. ISSN: 8756-3282. DOI: 10.1016/S8756-3282(01)00608-1.

[10] Ming Jer Hsieh et al. "Therapeutic potential of pro-angiogenic BPC157 is associated with VEGFR2 activation and up-regulation". In: *Journal of Molecular Medicine* 95 (3 2017), pp. 323–333. ISSN: 14321440. DOI: 10.1007/s00109-016-1488-y.

[11] Min Cheol Kim et al. "Cell Invasion Dynamics into a Three Dimensional Extracellular Matrix Fibre Network". In: *PLoS Computational Biology* 11 (10 2015). ISSN: 15537358. DOI: 10.1371/journal.pcbi.1004535.

[12] Alex Kiselyov, Konstantin V. Balakin, and Sergey E. Tkachenko. *VEGF/VEGFR signalling as a target for inhibiting angiogenesis*. Jan. 2007. DOI: 10.1517/13543784.16.1.83. URL: https://www.tandfonline.com/action/journalInformation?journalCode=ieid20.

[13] Yen Ling Koon et al. "Enhanced Delta-Notch Lateral Inhibition Model Incorporating Intracellular Notch Heterogeneity and Tension-Dependent Rate of Delta-Notch Binding that Reproduces Sprouting Angiogenesis Patterns". In: *Scientific reports* 8 (1 Dec. 2018). ISSN: 2045-2322. DOI: 10.1038/S41598-018-27645-1. URL: https://pubmed-ncbi-nlm-nih-gov.tudelft.idm.oclc.org/29934586/.

[14] Maibritt Kretschmer, Daniel Rüdiger, and Stefan Zahler. *Mechanical aspects of angiogenesis*. Oct. 2021. DOI: 10.3390/cancers13194987. URL: https://www.mdpi.com/2072-6694/13/19/4987/htm%20https://www.mdpi.com/2072-6694/13/19/4987.

[15] Maibritt Kretschmer et al. "Matrix stiffness regulates Notch signaling activity in endothelial cells". In: *Journal of Cell Science* 136 (2 2023). ISSN: 14779137. DOI: 10.1242/jcs.260442.

[16] Clemens Kuhn and Sara Checa. “Computational modeling to quantify the contributions of VEGFR1, VEGFR2, and lateral inhibition in sprouting angiogenesis”. In: *Frontiers in Physiology* 10 (MAR 2019), p. 288. ISSN: 1664042X. DOI: 10.3389/FPHYS.2019.00288/BIBTEX.

[17] Eri Matsuo et al. “Substrate stiffness modulates endothelial cell function via the YAP-Dll4-Notch1 pathway”. In: *Experimental Cell Research* 408 (1 2021), p. 112835. ISSN: 10902422. DOI: 10.1016/j.yexcr.2021.112835. URL: https://doi.org/10.1016/j.yexcr.2021.112835.

[18] Donna J Page et al. “Positive Feedback Defines the Timing, Magnitude, and Robustness of Angiogenesis”. In: (2019). DOI: 10.1016/j.celrep.2019.05.052. URL: https://doi.org/10.1016/j.celrep.2019.05.052.

[19] Margriet M Palm et al. “Computational Screening of Tip and Stalk Cell Behavior Proposes a Role for Apelin Signaling in Sprout Progression”. In: (2016). DOI: 10.1371/journal.pone.0159478. URL: http://dx.doi..

[20] Sotiris A Prokopiou et al. “Integrative modeling of sprout formation in angiogenesis: coupling the VEGFA-Notch signaling in a dynamic stalk-tip cell selection”. In: (2016). URL: http://arxiv.org/abs/1606.02167.

[21] David Sprinzak et al. “Cis-interactions between Notch and Delta generate mutually exclusive signalling states”. In: *Nature* 465 (7294 2010), pp. 86–90. ISSN: 00280836. DOI: 10.1038/nature08959.

[22] Cynthia L Stokes, Douglas A Lauffenburger, and Stuart K Williams. “Migration of individual microvessel endothelial cells: stochastic model and parameter measurement”. In: (1991).

[23] Benedetta Ubezio et al. “Synchronization of endothelial Dll4-Notch dynamics switch blood vessels from branching to expansion”. In: *eLife* 5 (APRIL2016 Apr. 2016). ISSN: 2050084X. DOI: 10.7554/ELIFE.12167.

[24] Lakshmi Venkatraman, Erzsébet Ravasz Regan, and Katie Bentley. “Time to Decide? Dynamical Analysis Predicts Partial Tip/Stalk Patterning States Arise during Angiogenesis”. In: *PLOS ONE* 11 (11 Nov. 2016), e0166489. ISSN: 1932-6203. DOI: 10.1371/JOURNAL.PONE.0166489. URL: https://journals.plos.org/plosone/article?id=10.1371/journal.pone.0166489.

[25] Xiaohong Wang et al. “YAP/TAZ Orchestrate VEGF Signaling during Developmental Angiogenesis”. In: *Developmental Cell* 42 (5 Sept. 2017), 462–478.e7. ISSN: 18781551. DOI: 10.1016/j.devcel.2017.08.002.

[26] Bahti Zakirov et al. “Active perception during angiogenesis: Filopodia speed up Notch selection of tip cells in silico and in vivo”. In: *Philosophical Transactions of the Royal Society B: Biological Sciences* 376 (1821 2021). ISSN: 14712970. DOI: 10.1098/rstb.2019.0753.

A

VEGF Gradient Field Stability

The VEGF gradient field is described by the partial differential equation

$$\begin{aligned} \frac{\partial V_a(\mathbf{x},t)}{\partial t} &= d\Delta V_a - k_{deg}V + V_{in}1_{\mathbf{x}=(x_p,y_p)}, && \mathbf{x}\in\Omega, \\ V_a(\mathbf{x},t) &= 0, && \mathbf{x}\in\delta\Omega, \\ V_a(\mathbf{x},0) &= 0, && \mathbf{x}\in\Omega\cup\delta\Omega, \end{aligned}$$

where Ω is the square of $0 < x < 1010\ \mu m$ and $0 < y < 1010\ \mu m$.
Discretizing this in the x and y-direction with a central difference scheme into equal parts of length $h = 10\ \mu m$ gives a system of the form

$$\begin{aligned} \frac{d\mathbf{u}}{dt} &= \mathbf{K}\mathbf{u} + \mathbf{r}, \\ \mathbf{u}(0) &= \mathbf{0}, \end{aligned}$$

where $u_{i,j}(t)$ denotes the numerical approximation of $V_a(\mathbf{x},t)$ and an internal point is approximated by

$$\frac{du_{i,j}}{dt} = d\frac{1}{h^2}(u_{i-1,j-1} + u_{i,j-1} - 4u_{i,j} + u_{i+1,j} + u_{i,j+1}) - k_{deg}u_{i,j} + V_{in}1_{(i,j)=(i_p,j_p)}.$$

The Gershgorin circle theorem says that the eigenvalues of a general $n \times n$ matrix **A** are located in the complex plane in the union of circles

$$|z - a_{i,i}| \leq \sum_{\substack{j\neq i \\ j=1}}^{n} |a_{i,j}|, \quad z \in \mathbb{C}.$$

For the non-boundary cases it follows that

$$\begin{aligned} &|\lambda - (-4d\frac{1}{h^2} - k_{deg})| \leq 4\frac{d}{h^2} \\ \iff &-\frac{8d}{h^2} - k_{deg} \leq \lambda \leq -k_{deg}. \end{aligned}$$

The boundary cases give a weaker condition and are therefore not included.
The Forward Euler method is conditionally stable and therefore must satisfy $dt \leq -\frac{2}{\lambda_i}\forall i$. Since $|\lambda|_{max} = -\frac{8d}{h^2} - k_{deg}$, this condition becomes

$$dt \leq \frac{2}{\frac{8d}{h^2} + k_{deg}}. \tag{A.1}$$

B

Parameter Sensitivity θ_1, θ_2

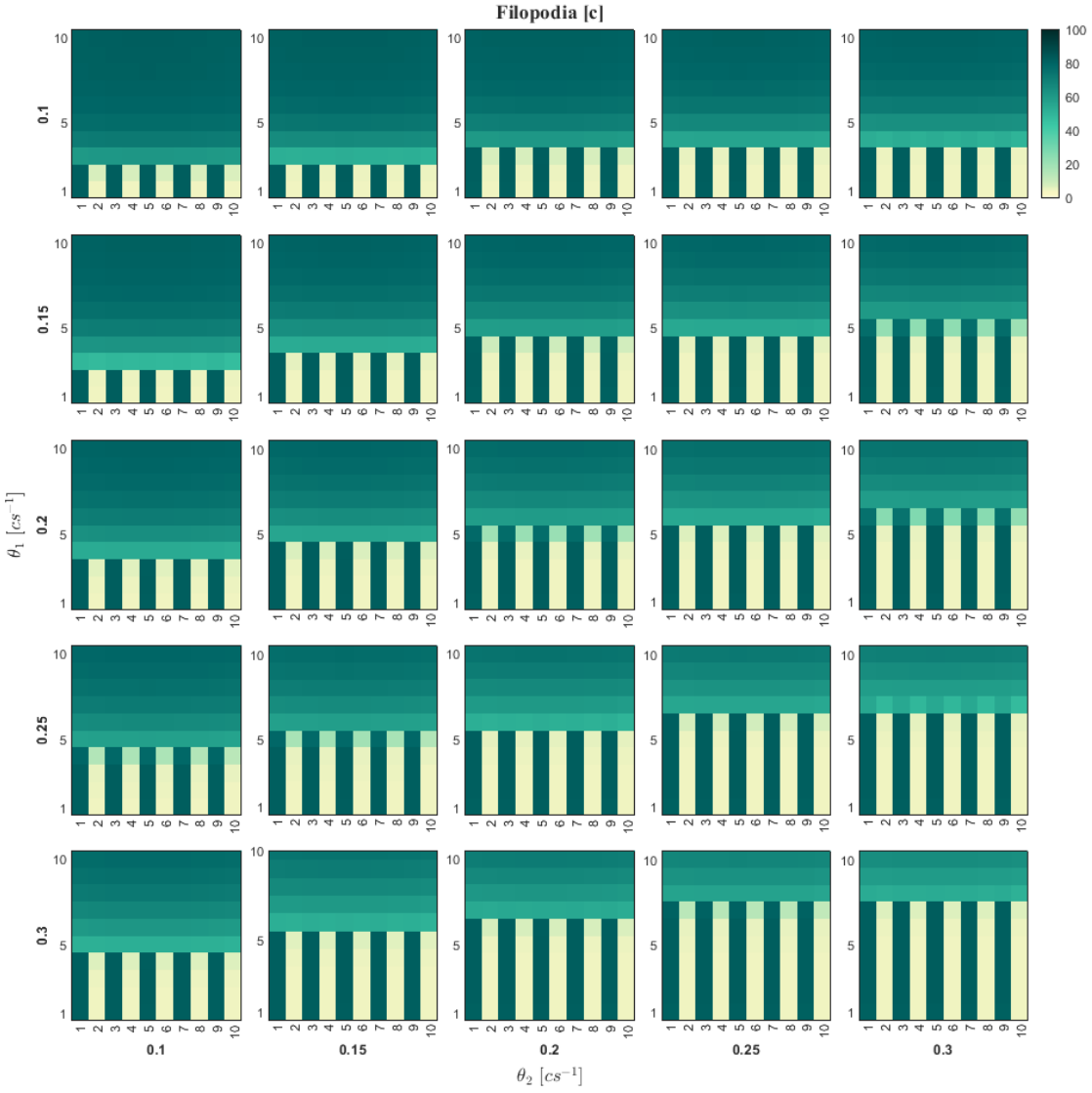

Figure B.1: Model predictions including Notch cleavage of the cell pattern in terms of filopodia concentration for ECM stiffness values from 1 to 10 kPa. This is done for various values of θ_1 (y-axis) and θ_2 (x-axis)